Supporting Information

Understanding and reducing photo-thermal forces for the fabrication of Au nanoparticle dimers by optical printing

Julian Gargiulo[1], Thomas Brick[2], Ianina L. Violi[1], Facundo C. Herrera[4], Toshihiko Shibanuma[2], Pablo Albella[2,3], Félix G. Requejo[4], Emiliano Cortes[2], Stefan Maier[2], Fernando D. Stefani[1,5]*

[1] Centro de Investigaciones en Bionanociencias (CIBION), Consejo Nacional de Investigaciones Científicas y Técnicas (CONICET), Godoy Cruz 2390, C1425FQD Ciudad de Buenos Aires, Argentina.

[2] The Blackett Laboratory, Department of Physics, Imperial College London, London SW7 2AZ, United Kingdom.

[3] University Institute for Intelligent Systems and Numerical Applications in Engineering (SIANI), University of Las Palmas de Gran Canaria, 35017, Las Palmas de Gran Canaria, Spain.

[4] Instituto de Investigaciones Fisicoquímicas Teóricas y Aplicadas (INIFTA), Dpto. de Química, FCE-UNLP, CONICET, La Plata 1900 Argentina.

[5] Departamento de Física, Facultad de Ciencias Exactas y Naturales, Universidad de Buenos Aires, Güiraldes 2620, C1428EAH Ciudad de Buenos Aires, Argentina.

***fernando.stefani@cibion.conicet.gov.ar**

SI.1 Optical printing set-up

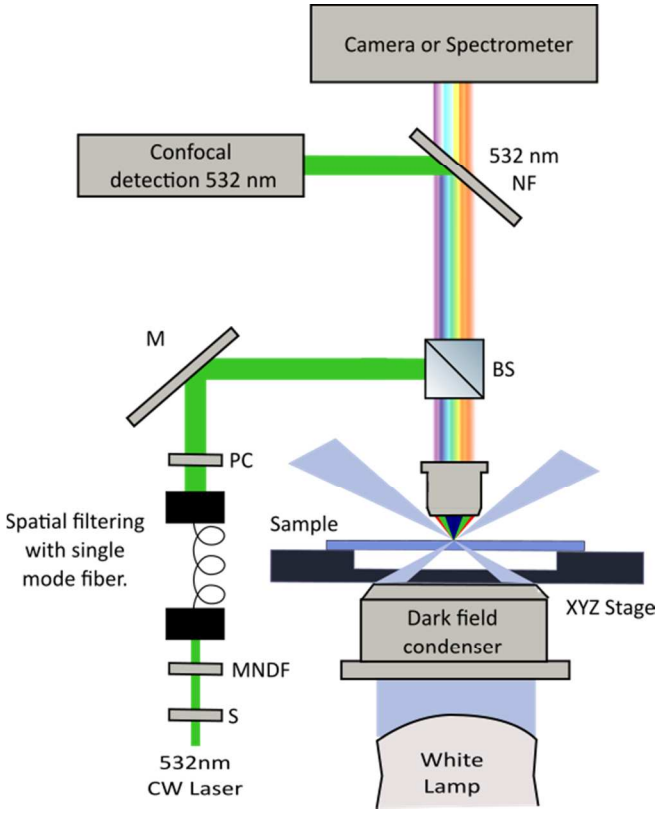

Figure S1. *Scheme of the experimental set-up. M:Mirror, BS:Beam Splitter, NF:Notch Filter, S: Shutter, MNDF: Motorized Neutral Density Filter. PC:Polarization control, consisting in a* $\lambda/2$ *and a* $\lambda/4$ *waveplate.*

The setup (schematically depicted in Figure S1), consists of a home-built upright optical microscope that combines Dark-field imaging in wide field with sample scanning confocal microscopy. Sample scanning is performed with an XYZ piezoelectric stage (PI P-545) with nanometer precision and a range of 200 μm in the three axes. A CW laser at 532 nm (Laserquantum Ventus) is used both for printing and as illumination source for confocal imaging. The beam is spatially filtered and its polarization is controlled using waveplates. The beam path includes a mechanical shutter and a neutral density filter mounted on a motorized flipper, both controlled from the computer. In this way the beam can be blocked, or its intensity switched between two values. The latter is useful when the same laser is used for both printing and scanning but different intensities are needed for each application.

SI.2 Dimers fabrication and characterization.

First, an extended grid of well separated NPs (at least 2 μm from each other) was fabricated by optical printing (see fig S2.a) or, in the case of the NDs, by electron beam lithography. Then, each NP on the array is localized and optical printing of a second NP was attempted in a position with a given set gap. Figure S2.b shows the same array after a second NP was printed, with a set gap of 440 nm. The fabrication process consists on the following steps:

1) The stage was moved so as to center the laser focus onto one of the NPs of the grid.
2) A 2D confocal image of the NP was acquired from which its precise location was obtained by computing the center of mass. The stage is moved to assure that the particle was centred with the printing beam.
3) The stage was then shifted to place the laser focus at the target position for the second NP. Then the printing beam was unblocked until the second NP was detected.
4) A confocal scan of the fabricated dimer was acquired.

The intensity was kept below the optical printing threshold during scanning steps. Light polarized perpendicularly to the dimer axis was used, in order to avoid a scattering signal from electromagnetically coupled NPs. Confocal scans are used to measure the experimentally obtained gap. An image of the isolated second particle is created (see figure S2.e), by subtracting the contribution of the first particle (acquired in step 2, figure S2.d) to the image of the dimer (acquired in step 4, figure s2.f). With this procedure, the position of each individual NP can be retrieved and the experimental gap can be computed.

Figure S2.g shows the measured gaps for each of the dimers shown in figure S2.b. Events where the second particle was not printed or looked significantly different (e.g. the reddish particle marked with a circle) were excluded from the analysis. In this example, the average achieved gap was (441 ± 10) nm.

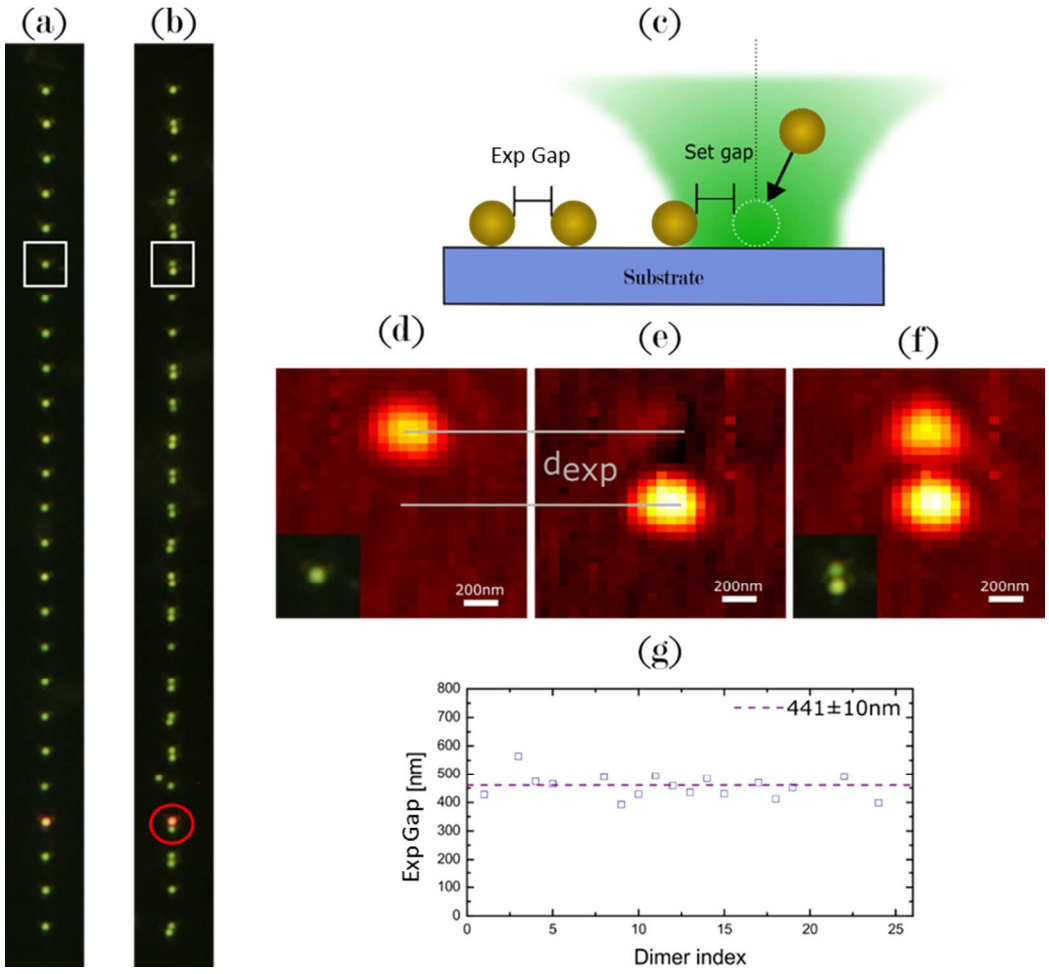

Figure S2. *(a) Dark field image of an array of Au 60nm NPs printed at* λ *=532 nm and P = 1.2 mW on glass (b) Dark field image of the same array after a second particle was printed. (c) Definition of the set gap d and the achieved experimental gap. (d) Confocal scan of the particle marked with a white box, acquired at* λ *= 532 nm and P = 0.4 mW before the printing of the second particle. Inset show the dark field image of the particle. (e) Image of the second particle built from the subtraction of images f and d. (f) Confocal scan of the dimer marked with a white box. Inset shown dark field image of the same dimer. (g) Obtained interparticle gaps. The mean value is* (441 ± 10) *nm.*

SI.3 Thermophoretic attraction to the substrate.

The observed threshold of laser power for optical printing a NP on sapphire is 2.4 times lower than on glass. The reason for this can be two-fold: i) The assembly process of polyelectrolytes can be different on sapphire, resulting in a lower superficial charge. ii) A short-ranged attraction between the heat-releasing particles and the heat-conductive surface is taken place. This self-induced thermophoretic force was theoretically introduced in a paper from Elperin[1] *et.al*. in 2003 and can be larger than the thermophoretic force caused by an external temperature gradient.

Elperin *et.al* claim that when a particle of radius a releases heat at a rate Q in a host medium of thermal conductivity κ_1 and is separated a distance z from a planar interface with another medium of thermal conductivity κ_2, a self thermophoretic force $\bar{F}_{stp}$ arises between the NP and the substrate given by

$$\bar{F}_{stp} = \frac{\pi\eta a\chi}{\kappa_1 z^2}\frac{\kappa_1-\kappa_2}{\kappa_1+\kappa_2} Q\ \hat{z} \qquad \text{(SI3.1)}$$

where $\hat{z}$ is the unit vector normal to the interface. If the thermal conductivity of the host medium is smaller than the one of the substrate, the force is attractive for heat-releasing particles.

Figure S3 shows the force for a 60 nm Au NP versus the distance to a sapphire substrate. The modulus of optical force when the NP is placed in the centre of the Gaussian beam is also shown for comparison. The attraction can be considerable strong for positions close to the substrate, contributing to print a NP, and probably explaining the lower laser power needed for printing on sapphire. Since this force, together with the electrostatic repulsion, are only active for short distances to the substrate (comparable to the diameter of the NPs), we did not include them in the discussion of the total force (figure 5 in the manuscript).

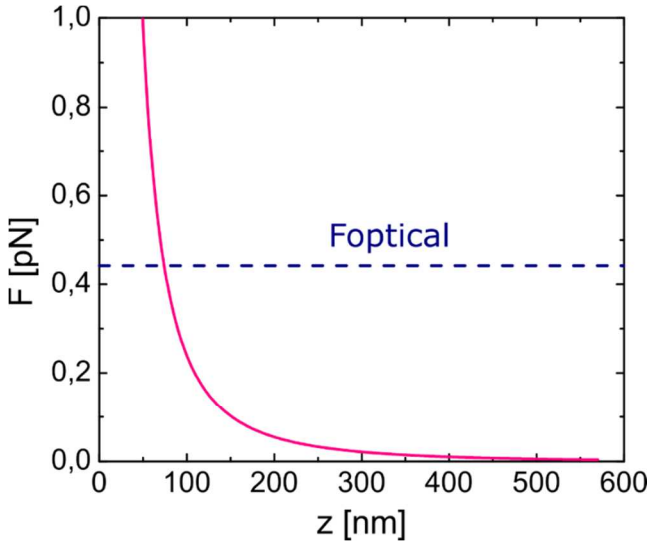

Figure S3. *Self-induced thermophoretic force acting on a 60 nm Au NP in water* ($\kappa_1 = 0.58\frac{W}{mK}$) *as a function of the distance to a sapphire substrate* ($\kappa_2 = 20\frac{W}{mK}$), *according to equation* SI3.1, *when the NP is in the centre of a Gaussian beam of* λ *= 532 nm with a waist w0 = 265 nm and P = 0.5 mW. The value of* $\chi = 10^{-10}\frac{m}{s^2}$ *was used. For comparison, blue horizontal line denotes the maximum optical force of a NP in the same beam.*

SI.4 Nano disks fabrication.

Gold ND were fabricated using electron beam lithography. Positive tone resist PMMA (poly(methyl methacrylate)) was coated on a sapphire substrate and baked at 180°C for 5 minutes. The substrate was exposed with an electron beam followed by a development procedure with MIBK (methyl isobutyl ketone): IPA (isopropanol) = 1:3 solvent. The nanostructured PMMA was covered with 2 nm chromium adhesion layer and 50 nm gold film deposited by thermal evaporation. Subsequent PMMA removal by lift-off process with acetone provided the gold nanodisks. Figure S4 shows representative dark field and SEM images of the fabricated disks.

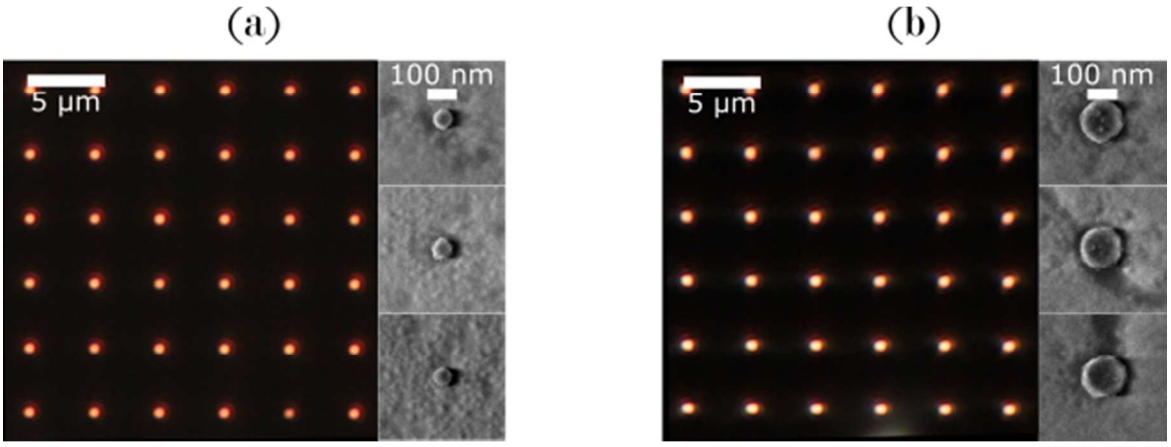

Figure S4. *(a) Dark field image of 70 nm NDs (b) and representative FE-SEM images of the structures (right) (b) Dark field image of 150 nm NDs (left) and representative FE-SEM images of the structures (right)*

SI.5 Optical properties of the ND

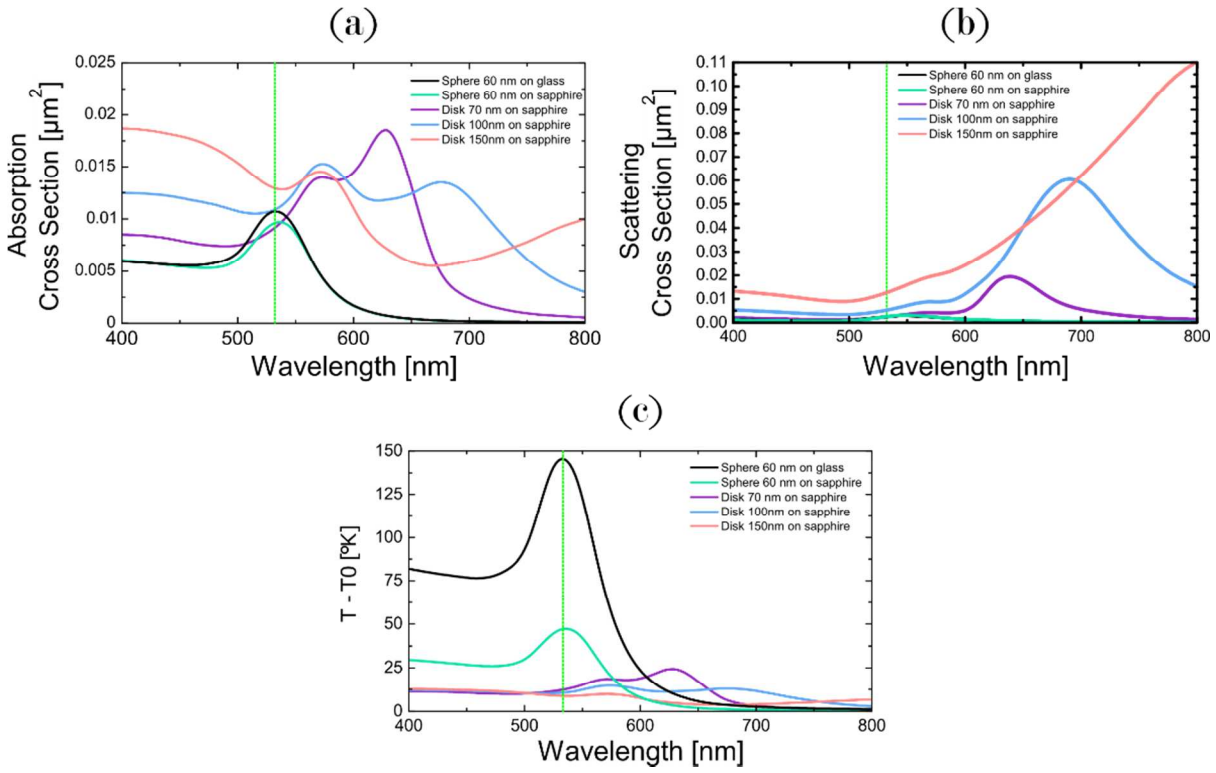

Figure S5: *Calculated absorption (a) and Scattering (b) cross-sections versus wavelength for AuNPs and AuNDs. (c) Calculated temperature increase of Au NPs and NDs versus wavelength under an irradiance of* $I = 4.6\ \frac{mW}{\mu m^2}$*, typical value for printing on sapphire at* λ*=532 nm. Calculations made solving the full heat diffusion equation with COMSOL software, as described in section SI.7*

SI.6 Optical force calculations.

Both for the calculations of temperature and optical forces, we considered our focused beam as Gaussian, propagating along the z direction:

$$E(r,z) = E_0\sqrt{\frac{2}{\pi}}\frac{w_0}{w}e^{\frac{-r^2}{w^2}}e^{i\left(k\left(\frac{r^2}{2R}+z\right)+\eta\right)}$$

$$R = z\left(1+\frac{z_0^2}{z^2}\right) \qquad \eta = \tan^{-1}\left(\frac{z}{z_0}\right) \qquad w(z) = w_0\sqrt{1+\left(\frac{z}{z_o}\right)^2}$$

where $k = \frac{2\pi n}{\lambda}$ is the wave-vector in the propagation medium of refractive index n. E_0 is the field amplitude at $(0,0)$, related to the total beam power through $|E_0|^2 = \frac{2P}{n\,c\,\epsilon_0 w_0^2}$. ϵ_0 is the permittivity of vacuum, c corresponds to the speed of light in vacuum, and $z_0 = \pi w_0^2\, n/\lambda$. The parameter w_0 is the beam waist at the focal plane (z = 0), also called the Gaussian beam radius, and represents the radius at which the field has decreased to 1/e, and the intensity has decreased to 1/e^2. w is the beam waist along the z direction and I_0 the time-averaged intensity at (0,0).

Gradient and scattering forces were calculated following the work by Agayan et al[2], according to:

$$F_{grad}^{z}(r,z) = -\frac{\varepsilon_0}{\pi}\alpha_{real}E_0^2\frac{zw_0^4}{z_0^2}\left(\frac{1}{w^4}-\frac{2r^2}{w^6}\right)e^{-\frac{2r^2}{w^2}}$$

$$F_{grad}^{r}(r,z) = -\frac{2\varepsilon_0}{\pi}\alpha_{real}E_0^2\frac{rw_0^2}{w^4}e^{-\frac{2r^2}{w^2}}$$

$$F_{sca}^{z}(r,z) = \frac{\varepsilon_0}{\pi}\alpha_{im}E_0^2\frac{w_0^2}{w^2}\left(k-\frac{kr^2}{2}\frac{z^2-z_0^2}{(z^2+z_0^2)^2}-\frac{w_0^2}{z_0w^2}\right)e^{-\frac{2r^2}{w^2}}$$

$$F_{sca}^{r}(r,z) = \frac{\varepsilon_0}{\pi}\alpha_{im}E_0^2\frac{rkw_0^2}{Rw^2}e^{-\frac{2r^2}{w^2}}$$

The polarizability $\alpha = \alpha_{real} + i\alpha_{im}$ was calculated using Kuwata expression.[3]

$$\alpha = V \frac{1 - \frac{1}{10}(\varepsilon + \varepsilon_m)x^2}{\left(\frac{1}{3} + \frac{\varepsilon_m}{\varepsilon - \varepsilon_m}\right) - \frac{1}{30}(\varepsilon + 10\varepsilon_m)x^2 - i\frac{4\pi^2\epsilon_m^{3/2}}{3}\frac{V}{\lambda^3}}$$

where V is the volume of the sphere, $x = \frac{2\pi na}{\lambda}$ is the size parameter and ε and ε_m are the dielectric function of the particle and the medium, respectively.

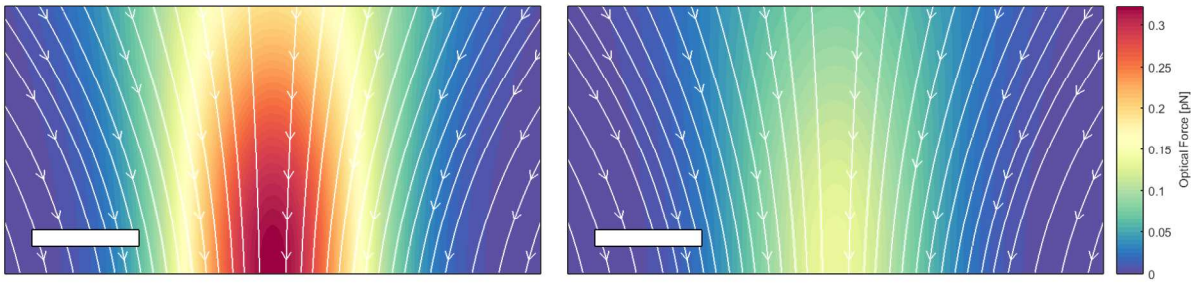

Figure S6: *Calculated optical forces using Gaussian laser printing beam of irradiance (left)* $I = 10.4\ \frac{mW}{\mu m^2}$*, as used when printing on glass substrate, and (right)* $I = 4.6\ \frac{mW}{\mu m^2}$*, as used when printing on sapphire. Optical force is defined as the sum of the gradient and the scattering forces. Focal plane is the bottom line of the figures. Streamlines indicate the direction of the total optical force, and the color scale indicates the magnitude. Scale bar: 200 nm.*

SI.7 Temperature calculations.

Upon illumination by a monochromatic light at angular frequency ω, a structure on the substrate will produces a heat source density proportional to the electric field intensity and the imaginary part of the material permittivity, ε:

$$q(\boldsymbol{r}) = \frac{\omega}{2} Im[\varepsilon] |\boldsymbol{E}(\boldsymbol{r})^2| \quad \text{(SI7.1)}$$

where the complex amplitude of the electric field, $\boldsymbol{E}(\boldsymbol{r})$ is given by $\boldsymbol{E}(\boldsymbol{r}, t) = Re\left[\boldsymbol{E}(\boldsymbol{r}) e^{-i\omega t}\right]$. Though the heat source is non-uniform, when considering gold structures in water, the large difference in thermal conductivities means we can adopt the uniform-temperature approximation[4] and the temperature profile inside the gold structure becomes homogeneous.

The temperature of the structures and the supporting substrate in the steady state may then be determined through the heat diffusion equation:

$$\rho C_p \nabla \cdot (T\, \bar{U}) = \kappa \nabla^2 T + q(r) \quad \text{(SI7.2)}$$

where ρ, C_p, and κ are the density, the heat capacity at constant pressure, and the thermal conductivity of the material, respectively, and $\bar{U}$ is the velocity field. The convective term $\nabla \cdot (T\, \bar{U})$ can be neglected here, because heat transfer in the nanoscale is dominated by conduction (see Donner et.al.[5] for details). In this way, temperature calculation is decoupled from fluid motion calculations. It can be resolved first, and the resulting temperature field be used to calculate fluid motion (see SI.8).

Numerical study of the temperature profiles were performed using COMSOL Multiphysics finite element modelling software. Full 3D simulations were conducted to solve equations S7.1 and S7.2 simultaneously.

The function $q(\boldsymbol{r})$, given by equation S7.1 , represents an energy (heat) source coming from light dissipation (EM losses) in the materials. Here, we assumed the EM losses from the light-matter interaction as the only heat source. To take into account heat dissipation in our simulation area, we implement a heat flux node across the outer boundaries, defined by the equation $q_0 = h(T - T_{ext})$, where h is the heat transfer coefficient of each medium,

dependent on the geometry, material and the ambient flow conditions, T_{ext} is the external temperature (assumed to be the same as the initial temperature of the system), and T is the temperature of the system. The heat transfer coefficient h can often be estimated by dividing the thermal conductivity of the convection fluid by a length scale. The permittivity of gold was taken from Johnson & Christy[6], while the remaining temperature dependent material parameters were taken from the COMSOL library.

The beam intensity was varied within throughout the simulations to reflect the notion that at a predefined set-gap the particle already on the substrate would be illuminated with the tail of the Gaussian beam rather than with the peak intensity. Spatially, the intensity at the substrate surface varies as

$$I(r) = I_0 ex\,p\left(-\frac{2r^2}{w_0^2}\right) \qquad (S7.3)$$

where I_0 is the intensity at the centre of the beam, w_0 is the waist radius determined as 266 nm for the 532 nm laser in use here, and r is the radial distance from the centre of illumination. As such, the temperature increase of the nanoparticles under illumination with the Gaussian tail is smaller than the expected increase had that particle been illuminated at a zero set-gap.

SI.8 Natural Convection and Thermo-Osmotic flow calculations.

The Navier-Stokes equation governs the stationary fluid velocity $\mathbf{v}$ profile as a result of the previously described temperature increase:

$$(\mathbf{v}(\boldsymbol{r}) \cdot \nabla)\mathbf{v}(\boldsymbol{r}) = \eta \nabla^2 \mathbf{v}(\boldsymbol{r}) + \boldsymbol{F}(T) \qquad (S8.1)$$

where η is the kinematic viscosity, and $\boldsymbol{F}(T)$ is the buoyancy force per unit mass due to temperature non-uniformity and, using the Boussinesq approximation[5], takes the form

$$\boldsymbol{F}(T) = \beta(T) g \Delta T \hat{\boldsymbol{z}} \qquad (S8.2)$$

where β is the volumetric expansion coefficient of water and g is gravitational acceleration. A fundamental characteristic in the analysis of fluid flow is the Reynolds number, which denotes the ratio between inertial and viscous forces:

$$Re = \frac{\tilde{U}\,\tilde{L}}{\eta} \qquad (S8.3)$$

where $\tilde{U}$ and $\tilde{L}$ are the characteristic velocity and length scales of the fluid motion, respectively. Taking a length scale of 60 nm (the diameter of nanoparticle in the printing experiments) and $\eta = 10^{-6}\, m^2 s^{-1}$, $Re \approx \tilde{U}\, 6.10^{-2}\, \frac{s}{m}$ which is $\ll 1$ for any physically meaningful velocity during the optical printing process. Such a low Reynolds number allows us to neglect the inertial term in the Navier-Stokes equations and treat the fluid as undergoing Stokes flow.

$$-\eta \nabla^2 \mathbf{v}(\boldsymbol{r}) = \boldsymbol{F}(T) \qquad (S8.3)$$

By calculating the orders of magnitudes of the diffusive and force terms of equation$S8.3$, we may estimate the characteristic velocity length scale for natural convection:

$$\tilde{U}_c \approx \frac{\beta g \Delta T}{\eta} \tilde{L}^2 \qquad (S8.4)$$

Using a temperature increase of approximately 100 K (see Fig 1A), $\beta = 10^{-4}\,\mathrm{K}^{-1}$, $g = 10\,\mathrm{ms}^{-2}$, $\eta = 10^{-6}\,\mathrm{m}^2\mathrm{s}^{-1}$ and $\tilde{L} = 60$ nm, we obtain a characteristic velocity of 0.3 nm s^{-1}.

The drag force $\bar{F}_d$ exerted on a suspended particle of radius a in a moving fluid is estimated by Stokes law

$$\bar{F}_d = 6\pi\mu a \bar{\mathrm{U}}_c \qquad (S8.5)$$

In order to calculate the thermo-osmotic flow field, numerical simulations using COMSOL were performed. First, the temperature maps were calculated, as described in section SI.7. Then, the slip velocity $\bar{U}_s$ was obtained according to

$$\bar{U}_s \cdot \hat{t} = \chi \frac{\nabla T}{T} \cdot \hat{t} \qquad (S8.6)$$

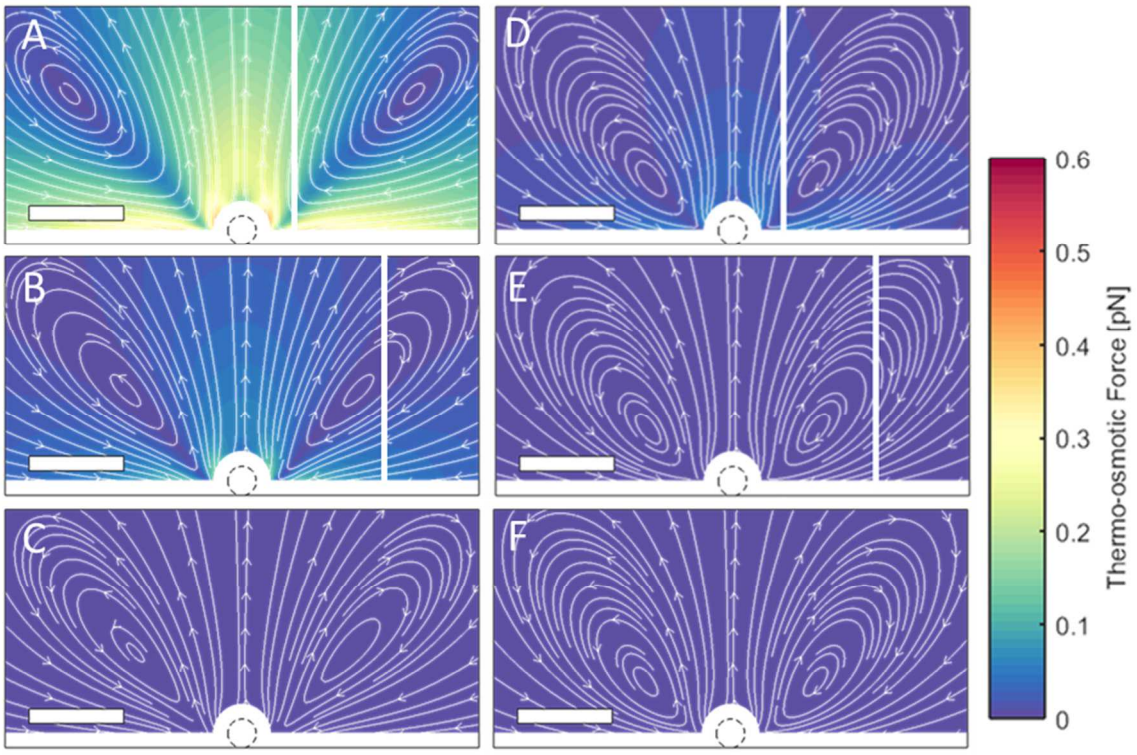

Figure S7: *Thermo-osmotic drag force on a 60nm AuNP in solution, around a 60nm AuNP illuminated with a Gaussian focus of* $w_0 = 266\ nm$, $\lambda = 532\ nm$, *on* ***(A-C)*** *glass substrate with* $I = 10.36\ mW\ \mu m^{-2}$ *and on* ***(D-F)*** *sapphire substrate with intensity* $I = 4.63\ mW\ \mu m^{-2}$. *Vertical lines indicate the center of the Gaussian focus:* ***(A,D)*** *50 nm set-gap;* ***(B,E)*** *240nm set-gap; and* ***(C,F)*** *450nm set-gap (out of figure axes range). Streamlines indicate the direction of the thermo-osmotic force, color scale indicates the magnitude. White masked regions indicate unphysical regions within which the 60nm printing particle would intersect the substrate or printed particle. Scale bar: 200 nm.*

This slip velocity was imposed as a boundary condition when solving the Navier-Stokes equation for stationary flows of low Reynolds (eq S8.3). Axial symmetry allowed us to reduce the simulation to 2D to study the velocity profile; COMSOL's heat transfer and microfluidic modules were used to solve equation S8.3. Both the spatial variation of the substrate temperature and the nanoparticle temperature were fixed to match those determined through

the 3D simulations described in section SI.7, while the open boundaries of the large simulation region ($100\ \mu m \times 50\ \mu m$) were set to room temperature. Once the thermo-osmotic velocity fields were calculated, they were translated into drag forces to a NP in solution using Stokes expression, (equation $S8.5$). The resulting Thermo-osmotic induced drag force maps can be seen in figures SI.7 and SI.8 for NPs and NDs respectively

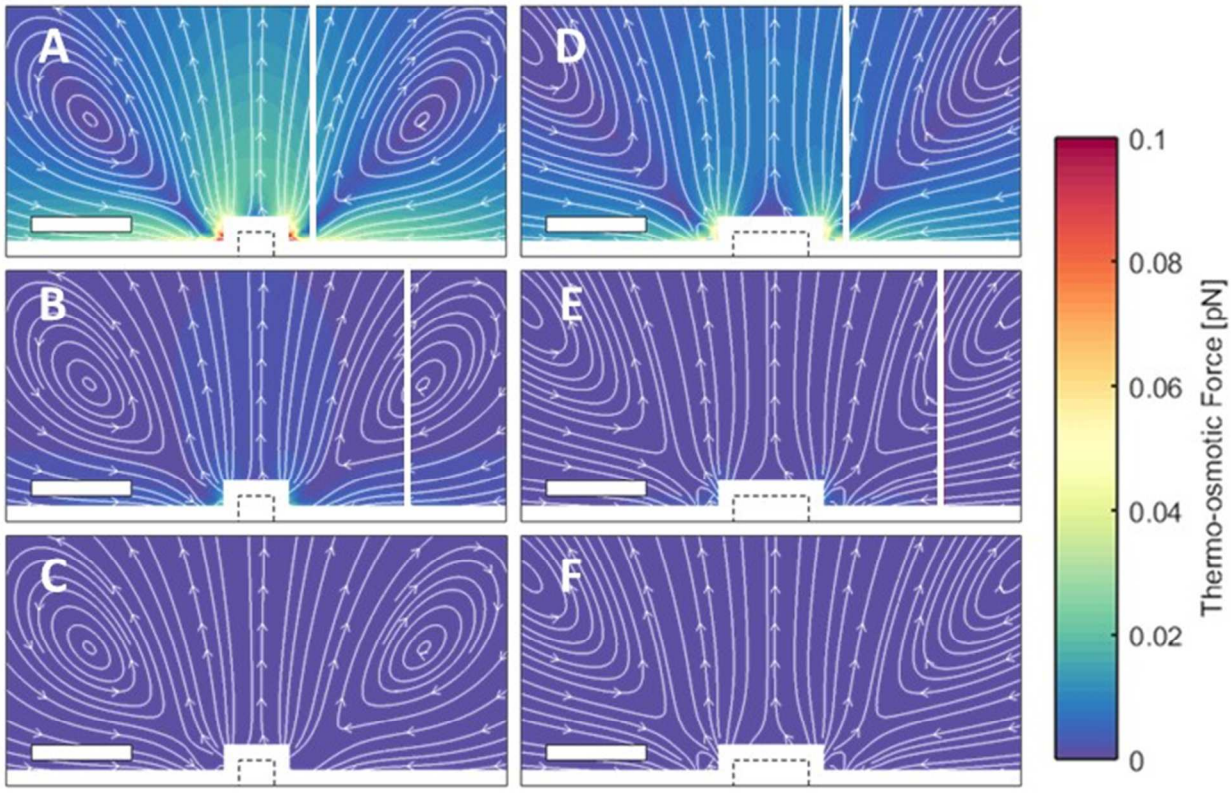

Figure S8: *Thermo-osmotic drag force on a 60nm AuNP in solution around a Au ND of 50 nm height and diameter of (**A-C**) 70nm, and (**D-F**) 150nm, on sapphire substrates. The NDs are illuminated with a Gaussian laser focus of* $w_0 = 266\ nm$, $\lambda = 532\ nm$ *with intensity* $I = 4.63\ mW\ \mu m^{-2}$. *Vertical lines indicate the centre of the Gaussian focus: (**A,D**) 50nm set-gap, (**B,E**) 240nm set-gap, and (**C,F**) 450nm set-gap (out of figure axes range). Streamlines indicate the direction of the thermo-osmotic induced force, and the color scale indicates the magnitude. White masked regions indicate unphysical regions within which the 60nm printing particle would intersect the substrate or printed particle. Scale bar: 200 nm.*

SI.9 Thermophoretic force calculations

Thermophoretic forces were calculated based on temperature maps, using

$$F_{tph} = -6\pi\mu a D_T \nabla T \qquad \text{(S9.1)}$$

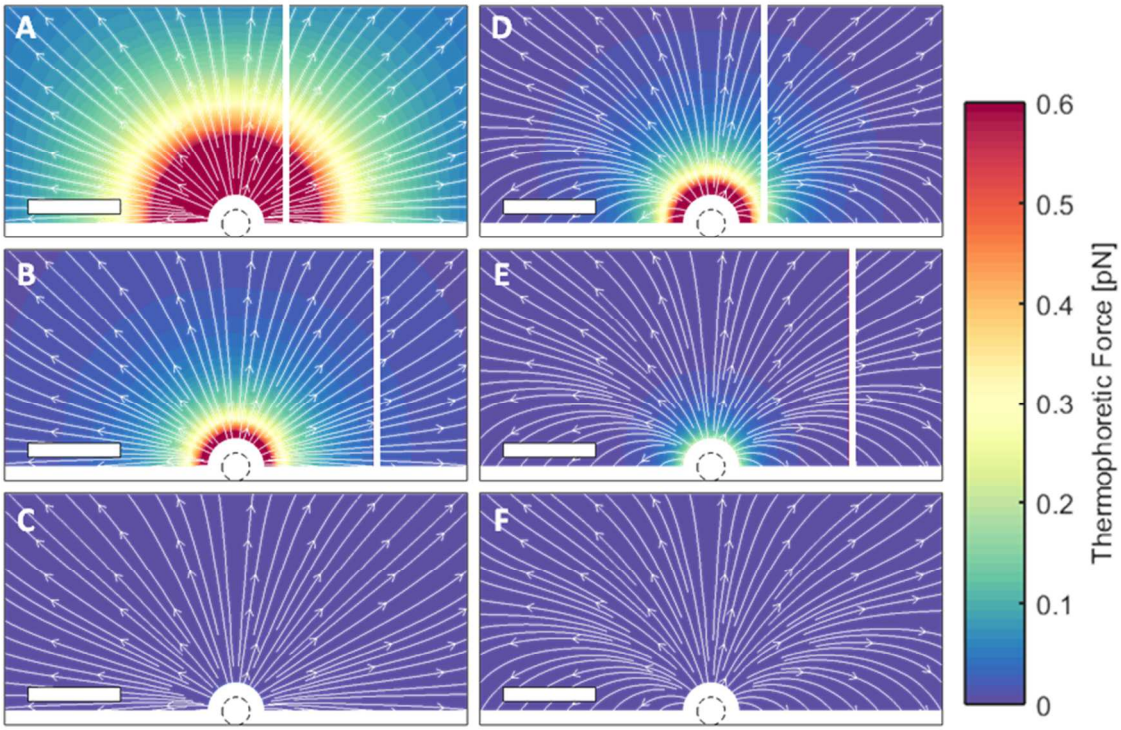

***Figure S9**: Thermophoretic force on a 60nm Au NP in solution around 60nm Au NP when illuminated with a Gaussian laser focus of w_0=266 nm, λ = 532 nm, on **(A-C)** a glass substrate with intensity I = 10.36 mW μm^{-2} and on **(D-F)** sapphire substrate with intensity I = 4.63 mW μm^{-2}. Vertical lines indicate the centre of the Gaussian focus: **(A,D)** 50nm set-gap; **(B,E)** 240nm set-gap; and **(C,F)** 450nm set-gap (out of figure axes range). Streamlines indicate the direction of the thermophoretic induced force, and the color scale indicates the magnitude. White masked regions indicate unphysical regions in within which the printing particle would intersect the substrate or printed particle. Scale bar: 200 nm*

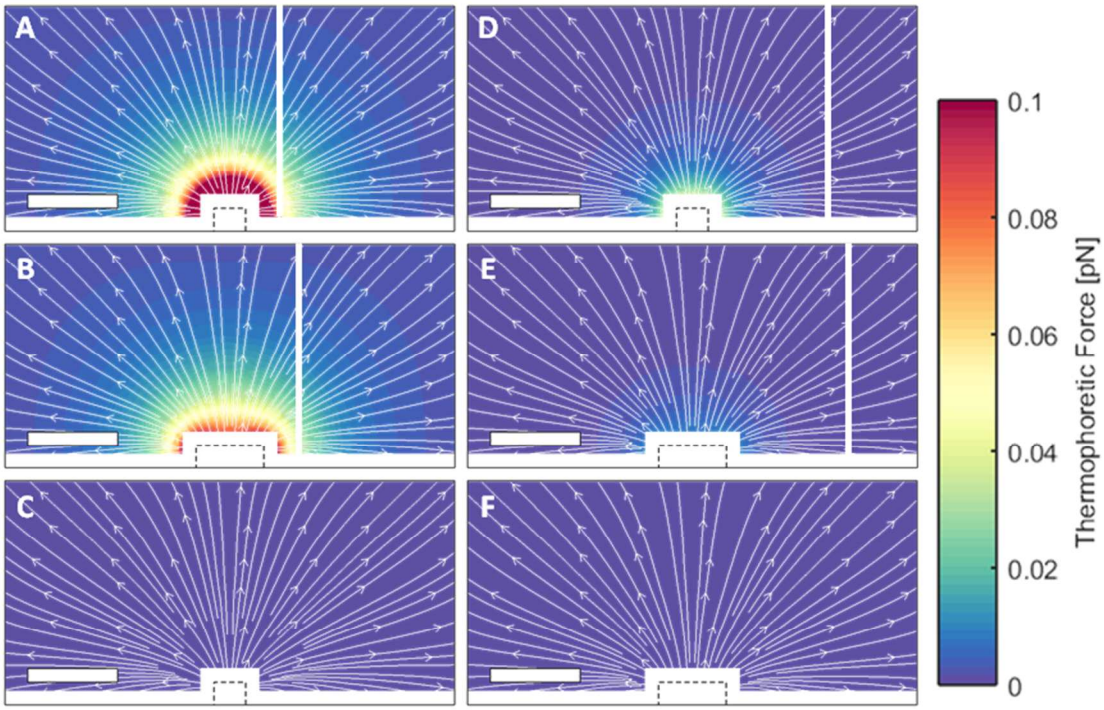

Figure S10. *Thermophoretic induced force on 60nm Au NP in solution around a ND of 50 nm height and diameter of (A-C) 70nm, and (D-F) 150nm, when illuminated with a Gaussian laser focus of* w_0*=266 nm,* λ *= 532 nm, on sapphire substrate with intensity I = 4.63 mW* μm^{-2}*. Vertical lines indicate the centre of the Gaussian focus: (A,D) 50nm set-gap; (B,E) 240nm set-gap; and (C,F) 450nm set-gap (beam out of range of figure axes here). Streamlines indicate the direction of the thermophoretic induced force, and the color scale indicates the magnitude. White masked regions indicate unphysical regions in within which the printing particle would intersect the substrate. Scale bar is 200 nm.*

SI.10 Parameter Optimization.

For each set of parameter (D_t, χ) we can calculate the total force map as the addition of three contributions: optical, thermophoresis and thermo-osmosis. Using the total force map, we can simulate a trajectory for the NP.

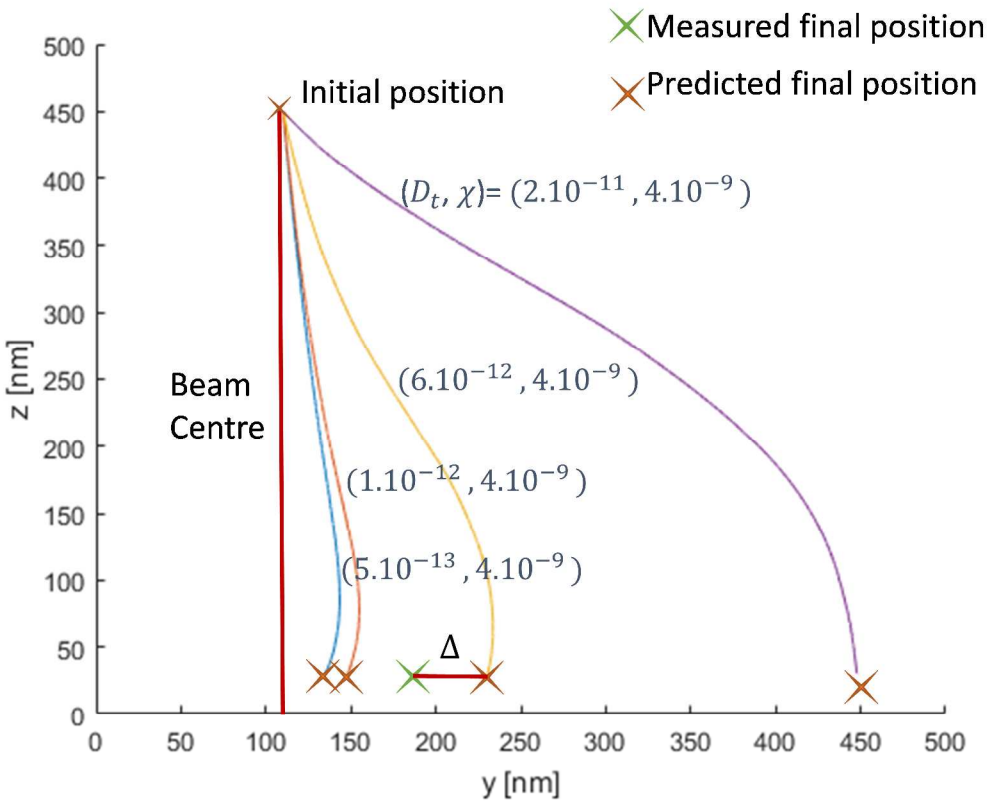

Figure S11: *Simulated trajectories of the NPs corresponding to different values of* (D_t, χ). *The red line indicate the position of the center of the beam. Green star mark the measured position and blue lines the predicted position for each set of parameter. Distance between both is the error* Δ.

We repeated this estimations for many pairs of (D_t, χ) and we calculated the error matrix Δ for each trajectory, as shown in figure SI.12

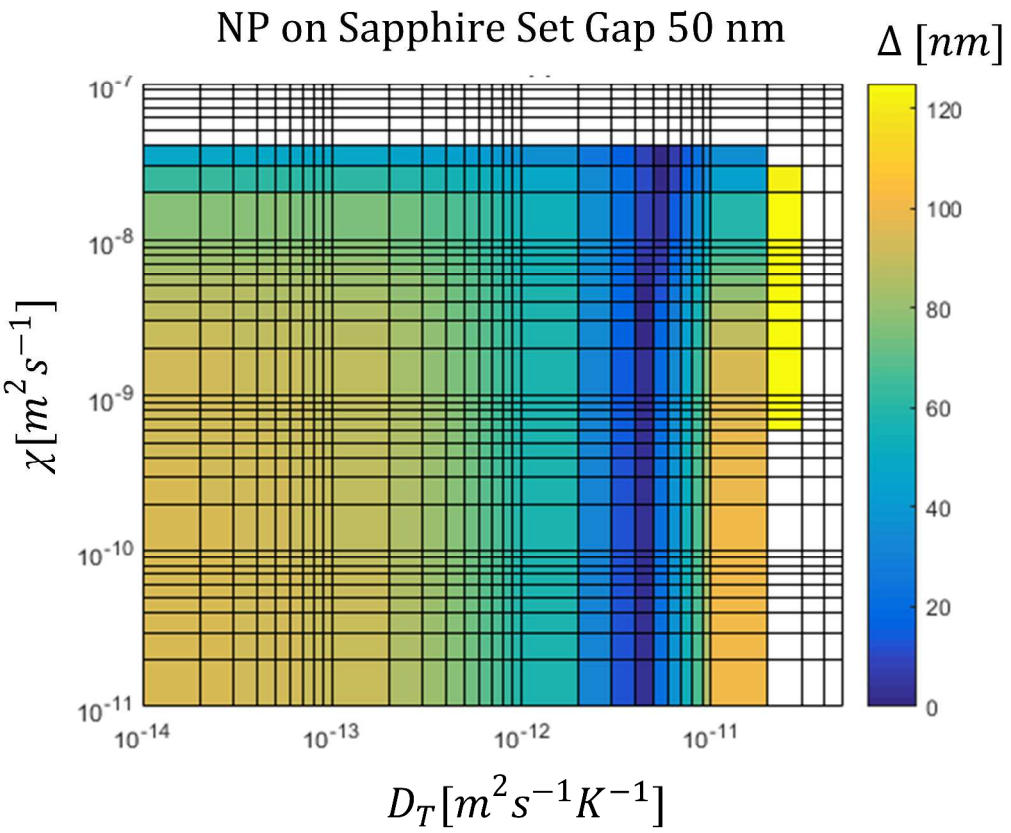

Figure S12: *Predicted error Δ as a function of parameters (D_T,χ) for a NP on sapphire and a set gap of 50nm. White squares means that final position of the trajectory is not on the substrate.*

Then we added the set of matrixes *Δ* corresponding to each experimental condition, including NP on glass and sapphire and to ND on sapphire for every set gap to find the cumulated *Δ*. As shown in figure SI.13 The minimum cumulated *Δ* is found for (D_T,χ)= $(4.3\ 10^{-12} m^2 s^{-1} K^{-1}, 3\ 10^{-9} m^2 s^{-1})$.

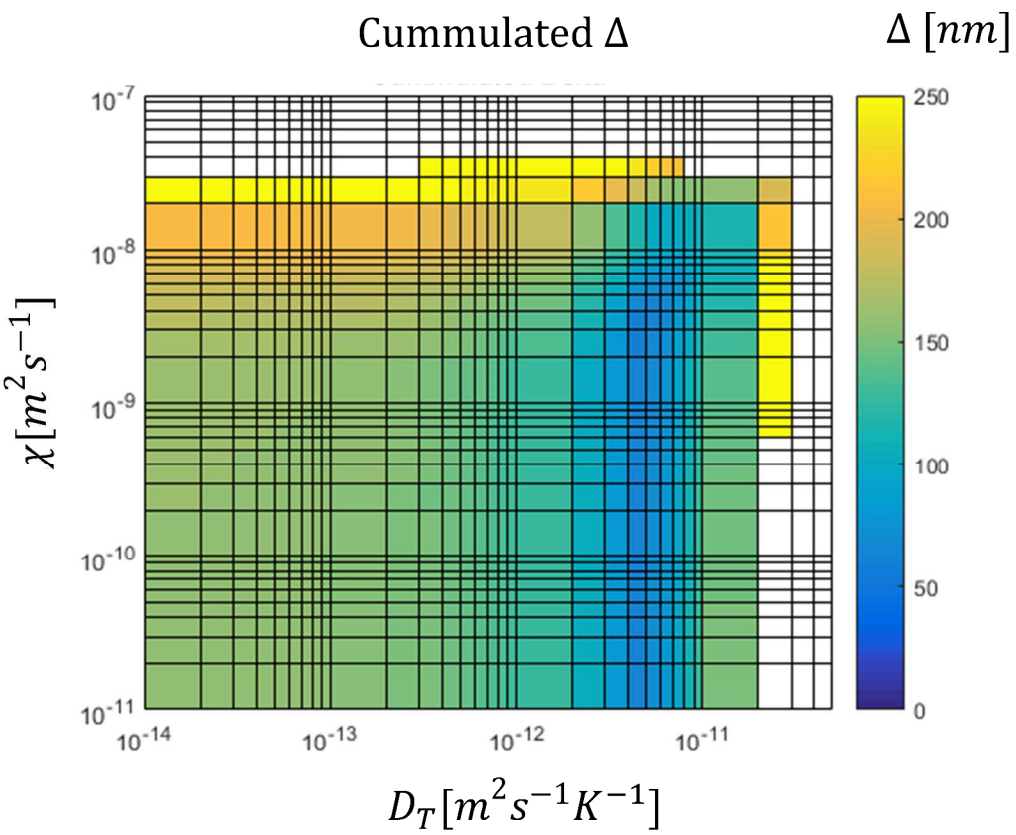

Figure S13: *Cumulated Δ as a function of parameters (D_T,χ). White squares means that final position of the trajectory is not on the substrate. Minimum Δ correspond to (D_T,χ)=* $(4.3\ 10^{-12} m^2 s^{-1} K^{-1}, 3\ 10^{-9} m^2 s^{-1})$

SI.11 Preparation of graphene substrates.

We used a Langmuir–Blodgett trough for the deposition of graphene oxide (GO) on a sapphire substrate, which was then treated in High Vacuum (HV) to obtain a negatively charged reduced graphene oxide (rGO) thin films. This way, a surface of rGO between one and two atomic layers of thickness, homogenously dispersed and chemically composed, was obtained with low a density of defects. An electronic conductivity as larger as 10^5 S/m was obtained on the same rGO thin film when on silicon. The homogeneity was tested by Raman and XPS spectroscopies at different regions of the sample.

Surface pressure measurements were performed using a Langmuir–Blodgett trough (KSV 5000, total area = 852 cm^2) at a symmetric compression rate of 10 mm min^{-1}. Langmuir films of graphene oxide (GO) were formed at the air–water interface by spreading, unless otherwise indicated, 3 ml of GO solution in methanol (1.0 mg ml^{-1}) using a Hamilton microliter syringe, on the MilliQ water subphase. The temperature was kept constant at (24 ± 1) °C, using a circulating water bath (Julabo, F12MC). Langmuir films were transferred onto silicon wafers treated with NH_4OH : H_2O_2 : H_2O (1 : 1 : 5), keeping the surface pressure constant by compression. The reduction treatment of GO to obtain the reduced GO films (rGO) was performed at 600 °C in a cylindrical furnace, with quartz tube, under high vacuum conditions.

REFERENCES

(1) Dolinsky, Y.; Elperin, T. *J. Appl. Phys.* **2003**, *93*, 4321–4327.

(2) Agayan, R. R.; Gittes, F.; Kopelman, R.; Schmidt, C. F. *Appl. Opt.* **2002**, *41*, 2318–2327.

(3) Kuwata, H.; Tamaru, H.; Esumi, K.; Miyano, K. *Appl. Phys. Lett.* **2003**, *83*, 4625–4627.

(4) Baffou, G.; Quidant, R.; García De Abajo, F. J. *ACS Nano* **2010**, *4*, 709–716.

(5) Donner, J. S.; Baffou, G.; McCloskey, D.; Quidant, R. *ACS Nano* **2011**, 5, 5457–5462.

(6) Johnson, P. B.; Christy, R. W. *Phys. Rev. B* **1972**, *6* , 4370–4379.